### Title

Comparative kinetic isotope effects on first- and second-order rate constants of soybean lipoxygenase variants uncover a substrate-binding network.




### Journal

Journal of Biological Chemistry, 294(48)



### Authors

Hu, Shenshen
Offenbacher, Adam
Lu, Edbert
et al.



### Publication Date

2019-11-29

### DOI

10.1074/jbc.RA119.010826

# Comparative kinetic isotope effects on first- and second-order rate constants of soybean lipoxygenase variants uncover a substrate-binding network

Received for publication, August 27, 2019, and in revised form, October 14, 2019 Published, Papers in Press, October 17, 2019, DOI 10.1074/jbc.RA119.010826

**Shenshen Hu**[‡¶1], **Adam R. Offenbacher**[‡¶‖], **Edbert D. Lu**[‡¶2], **and Judith P. Klinman**[‡§¶3]

*From the Departments of* [‡]*Chemistry and* [§]*Molecular and Cell Biology and the* [¶]*California Institute for Quantitative Biosciences (QB3), University of California, Berkeley, California 94720 and the* [‖]*Department of Chemistry, East Carolina University, Greenville, North Carolina 27858*

Edited by Ruma Banerjee

**Lipoxygenases are widespread enzymes found in virtually all eukaryotes, including fungi, and, more recently, in prokaryotes. These enzymes act on long-chain polyunsaturated fatty acid substrates (C18 to C20), raising questions regarding how the substrate threads its way from solvent to the active site. Herein, we report a comparison of the temperature dependence of isotope effects on first- and second-order rate constants among single-site variants of the prototypic plant enzyme soybean lipoxygenase-1 substituted at amino acid residues inferred to impact substrate binding. We created 10 protein variants including four amino acid positions, Val-750, Ile-552, Ile-839, and Trp-500, located within a previously proposed substrate portal. The conversion of these bulky hydrophobic side chains to smaller side chains is concluded to increase the mobility of flanking helices, giving rise to increased off rates for substrate dissociation from the enzyme. In this manner, we identified a specific "binding network" that can regulate movement of the substrate from the solvent to the active site. Taken together with our previous findings on C–H and $O_2$ activation of soybean lipoxygenase-1, these results support the emergence of multiple complementary networks within a single protein scaffold that modulate different steps along the enzymatic reaction coordinate.**

Understanding how enzymes work, especially with their vast rate enhancements of up to $10^{26}$-fold over uncatalyzed reactions, has been a continuous endeavor for enzymologists (1). Ever since the introduction of the Michaelis–Menten equation over 100 years ago, enzyme kinetic analysis has played a critical role in revealing the catalytic mechanisms of enzymes (2). Beginning in the 1970s, the integration of kinetic isotope effects (KIEs)[4] into the study of enzyme kinetics expanded the scope and insight derived from the classic Michaelis–Menten equation (3, 4). Some of the major applications of KIEs have been to determine the nature of rate-determining steps and to infer the nature of the chemical processes occurring within the enzyme active site (4–9). Most recently, in combination with various biophysical probes, patterns in KIEs at varied pressure and temperature have been utilized to investigate the link of protein motions to the chemical steps of catalysis (10–13).

Lipoxygenases are found to be widespread in plants, animals, fungi, and prokaryotes; the plant enzymes initiate the production of a spectrum of fatty acid hydroperoxides with key physiological roles in germination, growth, and senescence, as well as a defense response to pathogens (14, 15). One such enzyme, soybean lipoxygenase-1 (SLO), has emerged as a paradigmatic system for investigating enzymatic C–H activation reactions (16–20). Extensive kinetic studies of SLO under steady-state conditions have revealed a classic "ping-pong" mechanism in which a proton and electron are first irreversibly removed from one of its physiologically relevant substrates, linoleic acid (LA), by a nonheme iron center Fe(III)–OH, followed by the trapping of the substrate-derived radical by molecular oxygen (21). The C–H activation step has been concluded to dominate $k_{cat}$ at all temperatures, supported by the large (~80) and nearly temperature-independent $^{D}k_{cat}$ values for WT SLO (16, 17). Furthermore, it has been possible to link the properties of $k_{cat}$ to both local and global motions within the protein by comparing the properties of WT enzyme to a suite of mutations targeted at active site hydrophobic side chains (Leu-546, Leu-754, and Ile-553). The temperature dependence of $^{D}k_{cat}$ has been shown to be particularly informative (17–20, 22–24), indicating a more temperature-dependent $^{D}k_{cat}$ as the side-chain bulk at each of these positions is reduced. A mechanistic interpretation invokes a role for global conformational sampling in WT-SLO that leads to a precise alignment between the hydrogen donor (substrate) and acceptor (Fe(III)–OH). This property becomes

This work was supported by the National Institutes of Health Grants GM118117 (to J. P. K.) and GM113432 (to A. R. O.). The authors declare that they have no conflicts of interest with the contents of this article. The content is solely the responsibility of the authors and does not necessarily represent the official views of the National Institutes of Health.

This article contains Tables S1–S11.

[1] Present address: Corvus Pharmaceuticals, Inc., 863 Mitten Rd. #102, Burlingame, CA 94010.

[2] Present address: University of California, San Francisco, Helen Diller Family Cancer Research Bldg., 1450 3rd St., Rm. HD-220, MC 0520, San Francisco, CA 94158.

[3] To whom correspondence should be addressed: California Institute for Quantitative Biosciences, 608C Stanley Hall, UC Berkeley, Berkeley, CA 94720-3220. Tel.: 510-642-2668 or 510-643-5020; E-mail: klinman@berkeley.edu.

[4] The abbreviations used are: KIE, kinetic isotope effect; SLO, soybean lipoxygenase-1; LA, linoleic acid; H-HA, protio-LA; D-LA, perdeutero-LA; OS, oleyl sulfate; CHES, 2-(cyclohexylamino)ethanesulfonic acid; RP, reversed phase; HDX-MS, hydrogen deuterium exchange mass spectrometry.

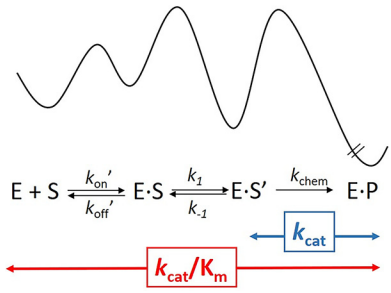


**SCHEME 1. Diagram to illustrate differences between first-order rate constants ($k_{cat}$) and second-order rate constants ($^{D}k_{cat}/K_m$) within the chemical reaction coordinate of SLO.** Given the sole rate limitation of $k_{cat}$ by the C–H abstraction step, $k_{cat}$ and $k_{chem}$, as well as $^{D}k_{cat}$ and $^{D}k_{chem}$, can be used interchangeably. The lack of the contribution of any steps preceding the formation of E·S′ to $k_{cat}$ indicates that $K = k_1/k_{-1} \gg 1$. Note that the size of the relative barriers for the conversion of E+S to E·S, E·S to E·S′, and E·S′ to E·P are for illustrative purposes only, to indicate the multiple partitionings between the forward and reverse steps that contribute to $k_{cat}/K_m$ but not $k_{cat}$. The magnitude of $k_{off}$ in the text and Table 3 refers to the net rate constant for release of the substrate from the stable E·S′ complex back to the free substrate and enzyme. For the model shown here, the magnitude of $k_{off}$ is approximated by $k_{-1}$.

compromised upon the decrease in volume at key active site residues, facilitating an onset of distance sampling along the hydrogen donor and acceptor coordinate to recapture the tunneling-ready distance characteristic of WT-SLO and an almost constant $^{D}k_{cat}$ (17–19, 23–25). The temperature dependence of $k_{cat}$ has also been identified as a possible indicator of perturbation-induced changes in global conformational sampling, in particular any change in the distribution of catalytically active protein substrates (22, 26). Note that the aforementioned kinetic investigations of SLO and their corresponding implications have been mainly focused on the first-order rate constants ($k_{cat}$) and related kinetic isotope effect value ($^{D}k_{cat}$) that fully represent the chemical transformation chemical step (Scheme 1), where $k_{cat} = k_{chem}$ (27).

Despite the emerging physical pictures that increasingly provide a resolved role for (local and global) motions that lead to productive reaction barrier crossings via hydrogen tunneling, a physical understanding of how SLO acquires and binds its long-chain fatty acid substrates has remained enigmatic (28, 29). One of the major reasons is a long standing inability to obtain X-ray structures of an enzyme–substrate complex (either with the natural substrate linoleic acid or a substrate analogue). A straightforward interpretation of kinetic isotope effects on the second order rate constant ($^{D}k_{cat}/K_m$) can be challenging compared with $^{D}k_{cat}$ because of the often complicating features of both substrate-binding and subsequent catalytic steps contributing to $k_{cat}/K_m$. As depicted in Scheme 1 for SLO, substrate binding can be conceptualized as an initial diffusional encounter (represented by $k_{on}'$ and $k_{off}'$), followed by substrate moving into and reorganizing within the long substrate-binding channel (represented by $k_1$ and $k_{-1}$). $k_{cat}/K_m$ reflects all steps up to and including the first irreversible step and thus includes the initial substrate binding (E+S ⇋ E·S), movement/reorientation of substrate after the initial substrate binding (E·S ⇋ E·S′), and the chemical step (E·S′ → E·P). Because the chemical step alone limits $k_{cat}$, $k_{-1}$ will be slower than $k_1$ (leading to the stable E·S′ complex in Scheme 1). Under the boundary conditions for $k_{cat}/K_m$ and $k_{cat}$ illustrated in Scheme 1, the observed off rate for substrate release, $k_{off}$, becomes equal to $k_{-1}$. The isotope effect on $k_{cat}/K_m$, $^{D}k_{cat}/K_m$, is shown in its generic form in Equation 1 and can be seen to be a function of $^{D}k_{cat}$, $k_{chem}$, and $k_{off}$, in which $k_{chem}$ and $k_{off}$ refer to the rate constants for the chemical step and the release of bound substrate back into solution, respectively (27, 30).

$$^{D}(k_{cat}/K_m) = (^{D}k_{cat} + k_{chem}/k_{off})/(1 + k_{chem}/k_{off}) \quad \text{(Eq. 1)}$$

The $^{D}k_{cat}/K_m$ values of WT SLO have been found to vary with temperature, changing from values much smaller than $^{D}k_{cat}$ at low temperature (<32 °C) to a value approximating $^{D}k_{cat}$ as the temperature is increased (27). As demonstrated by accompanying studies of viscosity, solvent isotope effects, and a pH profile at low temperature (<32 °C), the substrate diffusion to the active site, a subsequent rearrangement of preassociated substrate, and the chemical C–H activation are all concluded to be partially rate-limiting for protio-LA (H-LA), whereas the C–H activation becomes fully rate-limiting for the much slower perdeutero-LA (D-LA). Significantly, the addition of substrate mimics such as oleic acid and oleyl sulfate (OS) lead to an increase in $^{D}k_{cat}/K_m$ at 5 °C, approaching the value of $^{D}k_{cat}$; this result has implicated a regulatory site that causes the substrate to undergo more rapid dissociation (31). Similarly, in the absence of allosteric effectors, the C–H activation step also begins to fully dominate the $k_{cat}/K_m$ values for both H-LA and D-LA (>32 °C) (27). These different behaviors of the magnitude and temperature sensitivity of $^{D}k_{cat}$ and $^{D}k_{cat}/K_m$ are rich in mechanistic information. However, it is extremely difficult to tease out a meaningful physical model based solely on the data for WT SLO.

In the present study, results are provided that extend the investigation of $^{D}k_{cat}/K_m$ to a series of SLO variants that were predicted to have a possible impact on the efficiency of substrate release and/or binding to enzyme. As shown herein, whereas the kinetic features of certain SLO variants are essentially the same as WT, for a range of mutants the $^{D}k_{cat}/K_m$ value has become insensitive to changes in temperature. Four mutants, V750A, I552A, I839A, and W500F, are of particular interest, because of their generation of greatly elevated values for $k_{off}$ relative to WT. These four residues are located proximal to two helixes previously proposed to be important structural elements within the substrate portal (32, 33). These new data provide strong support for the previously defined substrate entry point, as well as identifying a new long-range network that modulates the movement of substrate to or from the solvent interface. The data highlight the valuable information content inherent to KIEs reflected in $k_{cat}/K_m$ and offer a new tool for understanding substrate-binding pathways.

## Results

WT SLO and 10 other variants, either bordering the proposed substrate-binding site (W500F, I538A, I552A, I553A, L546A, V750A, L754A, I553A, and I839A) (28) or at the predicted substrate entrance portal (E256A) (34), were chosen for the current investigation. The values and temperature dependence of $k_{cat}$ and $^{D}k_{cat}$ were obtained through steady-state kinetics assay with H-LA and D-LA between 10 °C and 45 °C

**Table 1**
**The comparison between $^{D}k_{cat}$ and $^{D}k_{cat}/K_m$ in SLO variants in 0.1 M borate buffer (pH 9.0)**
Kinetic parameters $k_{cat}$ and $^{D}k_{cat}$ are obtained by UV-visible assay. $^{D}k_{cat}/K_m$ values are obtained through competitive assay.

| | | $k_{cat\text{-}H}$ | | $^{D}k_{cat}$ | | $^{D}k_{cat}/K_m$ | |
|---|---|---|---|---|---|---|---|
| Category | Enzyme | 10 °C | 40 °C | 10 °C | 40 °C | 10 °C | 40 °C |
| | | $s^{-1}$ | | | | | |
| Trend I | WT[a] | 227 (17) | 346 (8) | 66 (5) | 52 (1) | 22 (1) | 48 (3) |
| | E256A | 208 (10) | 336 (10) | 59 (3) | 55 (2) | 15 (1) | 48 (2) |
| | R707A | 114 (8) | 181 (4) | 61 (4) | 47 (1) | 13 (1) | 28 (2) |
| | I553A | 115 (3) | 153 (3) | 148 (5) | 77 (2) | 12 (1) | 57 (2) |
| Trend II | L546A | 1.91 (0.05) | 3.34 (0.04) | 131 (6) | 85 (3) | 64 (3) | 72 (3) |
| | L754A[b] | 0.162 (0.009) | 0.347 (0.016) | 106 (8) | 82 (6) | 63 (2) | 68 (3) |
| | I538A | 148 (4) | 191 (6) | 100 (3) | 65 (2) | 45 (1) | 58 (5) |
| Trend III | V750A | 179 (6) | 173 (7) | 62 (3) | 57 (3) | 50 (3) | 54 (2) |
| | I552A | 76 (3) | 80 (2) | 66 (3) | 60 (2) | 57 (1) | 52 (1) |
| | I839A | 84 (2) | 171 (3) | 62 (2) | 72 (2) | 45 (3) | 54 (3) |
| | W500F | 174 (6) | 250 (4) | 77 (3) | 61 (1) | 55 (2) | 60 (1) |

[a] $k_{cat}$ and $^{D}k_{cat}$ are from Ref. 25.
[b] $k_{cat}$ and $^{D}k_{cat}$ are from Ref. 17.

using a continuous spectroscopic assay, in which the formation of the product hydroperoxide is monitored at 234 nm ("Experimental procedures"). Uncertainty in the precise substrate concentration in individual UV-visible measurements of H-LA and D-LA can lead to errors in fitted $k_{cat}/K_m$ value and $^{D}k_{cat}/K_m$ values. To overcome this limitation, a competitive assay ("Experimental procedures") involving HPLC was used to measure the $^{D}k_{cat}/K_m$ at different temperatures. The final $k_{cat}$, $^{D}k_{cat}$, and $^{D}k_{cat}/K_m$ values at the lowest (10 °C) and close to highest temperature (40 °C) for WT and 10 mutants are summarized in Table 1.

Inspection of $^{D}k_{cat}/K_m$ and $^{D}k_{cat}$ as a function of temperatures indicates three unique trends. The representative SLO in trend I is WT (Fig. 1*A*), where $^{D}k_{cat}/K_m$ values rise from being much smaller than $^{D}k_{cat}$ at 10 °C toward $^{D}k_{cat}$ with the increasing temperature. The data generated from the current study are in alignment with previous reports from this laboratory (27) and Holman and co-workers (35). E256A and R707A behave essentially the same as WT in terms of the temperature effects on $^{D}k_{cat}$ and $^{D}k_{cat}/K_m$ (Table 1). The variant I553A also appears to conform to Trend I, with the caveat that the isotope effect on $k_{chem}$ has become much more temperature-dependent, which will dampen any increase in $^{D}k_{cat}/K_m$ that is due to changes in rate-determining steps. A clear divergence of behavior is seen for L546A, L754A, and I538A, for which the $^{D}k_{cat}$ values decrease with temperature, and the $^{D}k_{cat}/K_m$ is almost temperature-independent (Trend II) (Fig. 1*B*). These are due to a decrease in $^{D}k_{cat}$ that is accompanied by a faster increase in $k_{off}$ than $k_{chem}$ at elevated temperature (Equation 1). The final pattern, revealed for V750A, I552A, I839A, and W500F, is of special interest because both $^{D}k_{cat}$ and $^{D}k_{cat}/K_m$ are nearly temperature-independent and virtually identical (Trend III; Fig. 1, *C* and *D*). In this instance the temperature independence of $^{D}k_{cat}/K_m$ can be directly attributed to a relatively small contribution of $k_{chem}/k_{off}$ (Equation 1).

The previous study of WT suggested a shift in the rate-limiting step toward the chemical step, $k_{chem}$, as the explanation for the elevation of $^{D}k_{cat}/K_m$ with increasing temperature (27). To investigate whether the substrate diffusion step (E+S ⇋ E·S) remains partially rate-limiting in the Trend II and Trend III behaviors, the viscosity dependence experiments were performed on representative SLOs from Trend II (L546A) and Trend III (V750A, I552A) (pH 9.0) at 20 °C. The viscosigen effects on WT SLO were also reinvestigated as a control. As seen in Fig. 2, for WT SLO, the $k_{cat}/K_m$ decreased dramatically as the relatively viscosity increased, indicating a 50% diffusion control, consistent with previous studies (27, 35). In sharp contrast, the $k_{cat}/K_m$ values in L546A, V750A, and I552A are weakly sensitive or independent of the increasing viscosity, indicating that the diffusion of substrate to enzyme is not significantly rate-limiting for these variants.

The kinetic parameters for WT SLO and the targeted mutants were further analyzed with H-LA as substrate in $H_2O$ and $D_2O$ (20 °C) to assess whether a solvent-dependent step that is distinct from $k_{on}'$ and has been ascribed to $k_1$ and $k_{-1}$ (Scheme 1) (27) would be partially rate-limiting. The values reported in Table 2 were obtained under pH conditions in which the rates for $k_{cat}$ and $k_{cat}/K_m$ have plateaued, avoiding potential complications from an impact of $D_2O$ on p$K_a$ (27). The reported data are corrected for the small impact of $D_2O$ on solvent viscosity (see "Experimental procedures"). WT SLO shows a very small solvent isotope effect on $k_{cat}$ (close to unity) and a larger value on $k_{cat}/K_m$, consistent with the previous investigation (27). For comparison, the impact of L546A, I552A, and V750A on the solvent isotope effect for $k_{cat}/K_m$ appears to be within experimental error relative to WT, implying that the change in the kinetic features of $^{D}k_{cat}/K_m$ in these three mutants is unrelated to a solvent-dependent step.

To gain a more quantitative measure of the observed effects, changes in the commitment factor and $k_{off}$ (Equation 1) were calculated where relevant (Table 3). We note that decreases in computed $k_{off}$ values for substrate release can be accompanied by even greater decreases in $k_{cat}$ values. For example, compared with WT, the active site mutants L546A and L754A demonstrated 60- and 675-fold decreases in the $k_{off}$ compared with 180- and 2000-fold reductions for the C–H activation step. Thus, the commitment value, $k_{chem}/k_{off}$, provides a more accurate assessment of the shift in rate-limiting steps. As shown in Table 3, all seven mutants in Trend II and Trend III demonstrate a decreased commitment compared with WT, implicating a more efficient substrate release process in relation to changes in the C–H activation step. In particular, Trend III mutants (V750A, I552A, W500F, and I839A) show smaller commitment values than Trend II mutants (L546A, L754A, and

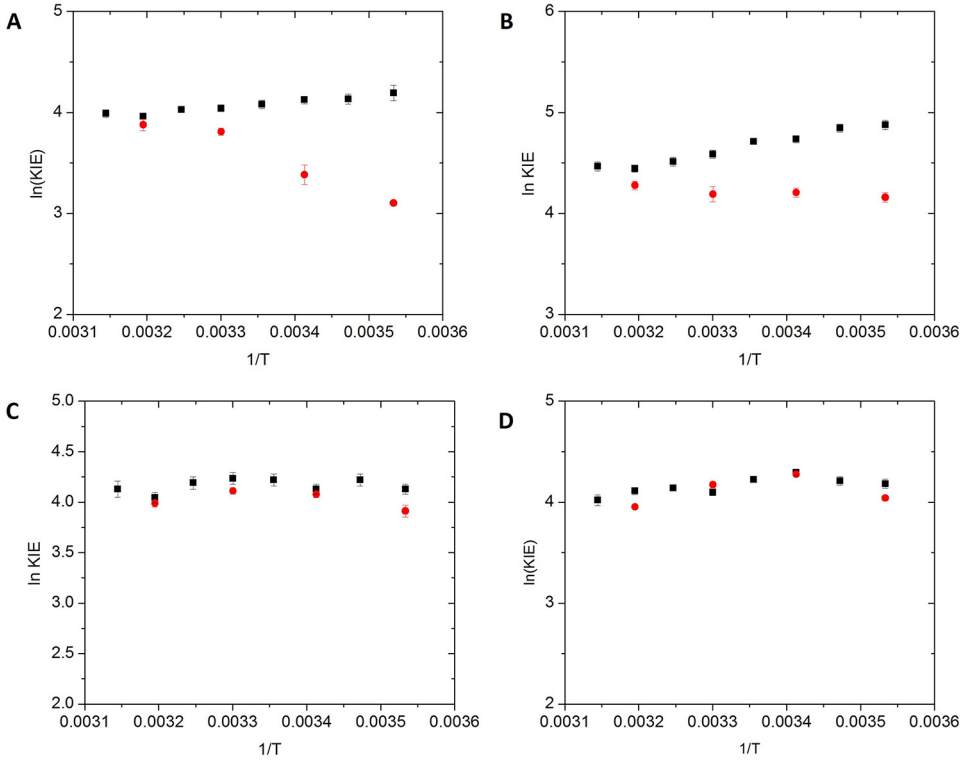


**Figure 1. Results of variable temperature $^{D}k_{cat}/K_m$ (*red circle*) and $^{D}k_{cat}$ (*black square*) with WT (*A*), L546A (*B*), V750A (*C*), and I552A (*D*).** The $^{D}k_{cat}/K_m$ values were obtained through competitive assay in 0.1 borate buffer (pH 9.0) whereas the $^{D}k_{cat}$ values were obtained through steady-state kinetics assays.

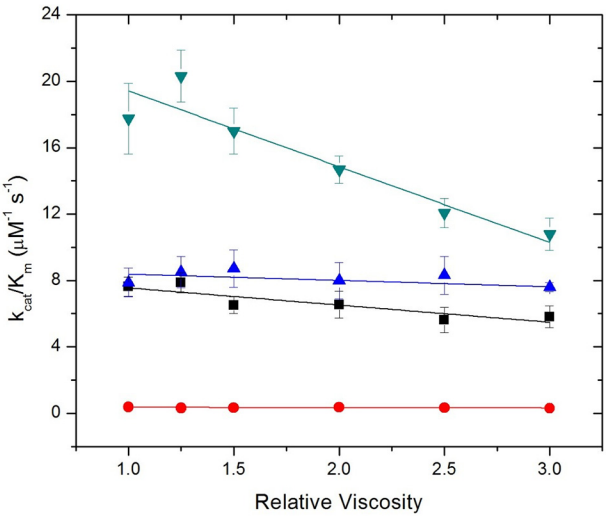


**Figure 2. Effect of viscosigen WT SLO (*cyan inverted triangles*), I552A (*blue triangles*), V750A (*black squares*), and L546A (*red circles*) in 0.1 M CHES buffer (pH 9.0) with glucose at 20 °C.**

**Table 2**

**Solvent isotope effect at 20 °C with H-LA**

$H_2O$ buffer contained 0.1 borate (pH 9.0) in $H_2O$. $D_2O$ buffer contained 0.1 M borate (with a pH meter reading of 8.6) in $D_2O$.

| Enzyme form | $k_{cat}$ | $k_{cat}/K_m$ |
|---|---|---|
| WT | 1.26 (0.07) | 1.70 (0.20) |
| I552A | 0.80 (0.02) | 1.51 (0.11) |
| L546A | 0.83 (0.02) | 1.56 (0.10) |
| V750A | 0.72 (0.11) | 2.40 (0.50) |

**Table 3**

**The commitment ($k_{chem}/k_{off}$) and $k_{off}$ value in SLO variants in 0.1 M borate buffer (pH 9.0) at 10 °C**

| | SLO | $k_{chem}/k_{off}$ [a] | $k_{off}$ [a] |
|---|---|---|---|
| | | | $s^{-1}$ |
| Trend I | WT | 2.1 (0.3) | 108 (16) |
| | E256A | 3.1 (0.3) | 66 (7) |
| | R707A | 4.0 (0.5) | 29 (4) |
| | I553A | 12.3 (1.2) | 9.30 (0.94) |
| Trend II | L546A | 1.1 (0.1) | 1.79 (0.20) |
| | L754A | 0.69 (0.13) | 0.16 (0.03) |
| | I538A | 1.3 (0.1) | 118 (8) |
| Trend III | V750A | 0.24 (0.08) | 718 (259) |
| | I552A | 0.16 (0.05) | 472 (167) |
| | I839A | 0.45 (0.09) | 185 (37) |
| | W500F | 0.40 (0.06) | 435 (73) |

[a] The $k_{chem}/k_{off}$ values and $k_{off}$ values are calculated from $^{D}k_{cat}/K_m$, $^{D}k_{cat}$, and $k_{cat}$ values through Equation 1. The errors are calculated on the basis of error propagation equations.

I538A), and an increased $k_{off}$ value relative to WT despite the 2–4-fold decrease in $k_{cat}$.

## Discussion

The synergistic analysis of mutagenesis, viscosity, and solvent and substrate isotope effects on $k_{cat}/K_m$ and $k_{cat}$ is able to tease apart the changes in rate limitation arising from the initial substrate-binding step (E+S ⇋ E·S), a subsequent reorientation/isomerization of the substrate (E·S ⇋ E·S′), and the chemical step (ES′ → EP; Scheme 1). Although the contribution from $D_2O$-related steps ($k_1$ and $k_{-1}$ in Scheme 1) is essentially the same in all the mutants, the substrate diffusion step ($k_{on}'$) is significantly less rate-limiting in the single mutants tested

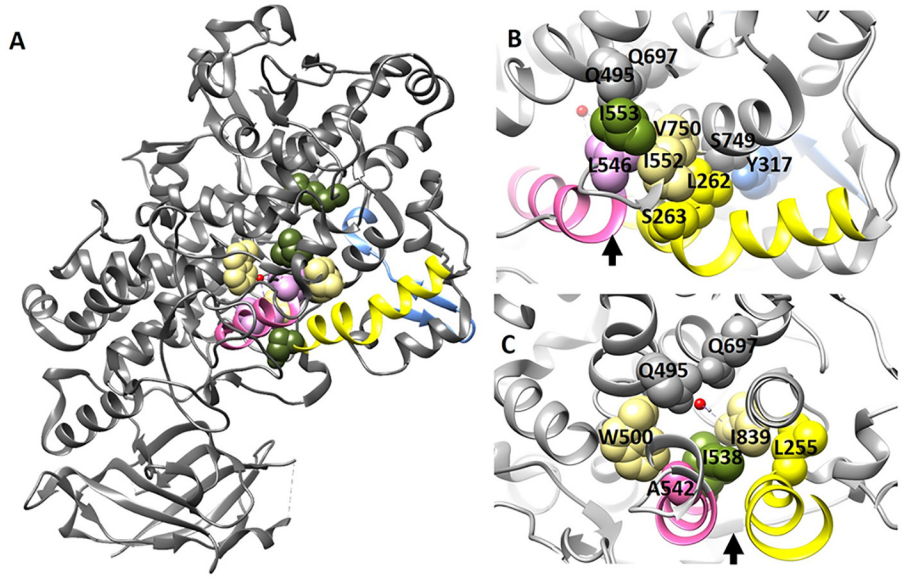


**Figure 3. X-ray structure of SLO (Protein Data Bank code 1F8N), with iron colored in *red*, Trend I residue (Glu-256, Arg-707, and Ile-553) colored *olive green*, Trend II residues (Leu-546, Leu-754, and Ile-538) colored *light purple*, Trend III residues (Val-750, Ile-552, Ile-839, and Trp-500) colored *khaki*, helix 2 highlighted by *yellow*, helix 11 highlighted by *pink*, and previously identified thermal activated remote loop 317–334 highlighted by *light blue* (25).** *A*, bird's eye view of mutated residues in this study, helices 2 and 11, and remote loop 317–334. *B*, two networks in SLO intersect at residues Val-750 and Ile-552. The Val-750 and Ile-552 are within the network that modulate the chemical steps across the surface loop 317–334, connector Ser-749, Tyr-317, and active site residues Ile-553 and Leu-546. The Val-750 and Ile-552 are also in contact with residues on the substrate portal helix 2. *C*, the residues Ile-839 and Trp-500 are in contact with residues on the substrate portal helix 2 and helix 11. The *black arrow* in each panel indicates the proposed substrate entrance between helix 2 and 11 (32, 33). Gln-495 and Gln-697 (colored *gray*) were proposed to be located around the binding pocket in an earlier study (35).

(L546A, V750A, and I552A). The comparison between $^{D}k_{cat}/K_m$ and $^{D}k_{cat}$ further indicates distinct kinetic features underlying the three mutants. In the cases of V750A and I552A, the almost identical $^{D}k_{cat}$ and $^{D}k_{cat}/K_m$ at low temperatures supports the conclusion that the C–H bond cleavage is the primary rate-limiting step for both $k_{cat}$ and $k_{cat}/K_m$. In contrast, the $^{D}k_{cat}/K_m$ value of L546A is half of the $^{D}k_{cat}$ value at 10 °C, clearly showing the presence of at least one additional kinetically limiting step beyond the substrate-binding and chemical step.

The commitment factors calculated from the $^{D}k_{cat}/K_m$ and $^{D}k_{cat}$ values are able to quantify the shifting of the rate-limiting step in $k_{cat}/K_m$ for SLO variants (Table 3). The commitment value in WT was calculated as 2.1 at low temperature, where the rate limitation is comprised of both C–H activation and substrate-binding/release steps; the three mutants that demonstrate Trend I kinetic features (E256A, R707A, and I553A) all show increased commitment factors, a result of $k_{off}$ decreasing more than $k_{chem}$. Conversely, the commitment factors in the Trend II and Trend III mutants all decrease (by 2–20 times compared with the WT). The smaller commitment factors in Trend II and Trend III relative to WT are consistent with the viscosity dependence results that indicate a decrease in rate limitation from the substrate diffusion step (see Fig. 2 for the representative Trend II mutant L546A and Trend III mutants V750A and I552A). Note that the commitment factors of the Trend III mutants are in general smaller than the Trend II mutants (Table 3), implying that the chemical step contributes the most to the rate limitation of $k_{cat}/K_m$ for the variant V750A, I552A, I839A, and W500F.

The extensive series of single mutants that display weak or no temperature dependence for $^{D}k_{cat}/K_m$ (Table 1) all feature a size reduction at a single hydrophobic side chain, either (i) close to the reactive iron (Leu-546 and Leu-754) (17), (ii) lining the putative substrate wall (Trp-500 and Ile-538) (36, 37), (iii) at the terminal carboxylate Ile-839 that serves as an active site iron ligand (38), or (iv) at two positions predicted to serve as a linchpin between the reactive carbon of substrate and a previously described dynamical network linking a surface loop to the active site (Val-750 and Ile-552) (25). In an earlier study, it was shown that size reduction in Gln-495 and Gln-697, two residues that serve as second-sphere ligands of the nonheme iron center and are located adjacent to the putative substrate-binding pocket (Fig. 3, *B* and *C*), both lowered the catalytic efficiency and eliminated the temperature sensitivity of $^{D}k_{cat}/K_m$ (35). The authors noted the need for close packing to properly position the substrate in relation to the active site iron, with the enlargement of the cavity leading to an impaired and more rate-limiting chemical step. Our results herein corroborate this previous proposal that the close packing of the SLO structure is crucial to the orientation of substrate and further provide more detailed information on how a protein network contributes to formation of the E–S complex.

In Trend II mutants, the size reduction of two positions (Leu-546 and Leu-754) occurs at side chains that are located in the center of the active site in WT SLO, adjacent to the iron cofactor and the reactive carbon of the linoleic acid. These have previously been shown to lead to a severely impaired chemical step (17). From Table 3 it can be seen that such mutations also give rise to large reductions on the $k_{off}$ values (60- and 675-fold, respectively). The expanded active site in these two mutants may provide more space for substrate binding with unfavorable conformers that impact both substrate release and C–H activation. Given the absence of a viscosigen effect for L546A (Fig. 2),

we propose that the reorientation of the substrate from its initially formed "inactive" complex to a catalytically competent and tight bending configuration(s) (E·S ⇋ E·S′) may have become partially rate-limiting in Trend II mutants. The previously generated double mutant of SLO (L546A and L754A) demonstrated the importance of a substrate reorientation steps, likely a consequence of the very significant increase in the active site cavity that gives rise to unfavorable initial binding of the substrate (39, 40). When taken together, the kinetic parameters of the double mutant that include a severely impaired $k_{chem}$, an almost temperature-independent $^{D}k_{cat}/K_m$ value of ~30–40 and a huge $^{D}k_{cat}$ value are also indicative of a reduced $k_{off}$ (30, 41).

The fact that the Trend III mutants V750A, I552A, W500F, and I839A demonstrate a large *increase* in $k_{off}$ values (Table 3) is of particular interest. As discussed above, residues at these four positions lie along the postulated substrate-binding pocket (28). Through a detailed examination of the WT SLO structure, we observe a large number of hydrophobic interaction between these four side chains on helix 2 (residues 255–275) and 11 (residues 535–545; Fig. 3*A*): side chains Val-750 and Ile-552 are in van der Waals contact with Leu-262 and Ser-263, correspondingly (Fig. 3*B*); the side chain Ile-839 is anchored in the middle of Leu-255 and Ile-538; Trp-500 is adjacent to residue Ala-542, which is also located on helix 11 (Fig. 3*C*). The early studies on SLO had proposed that substrate enters the binding site through a gap between helix 11 and helix 2. As shown from the present studies, reducing the residue size at Val-750, Ile-552, Ile-839, or Trp-500 causes a "loosening up" of the substrate portal, facilitating substrate binding (Fig. 2) and release (Table 3). It is worth noting that the single mutant at the substrate entrance (E256A on helix 2) does not increase the $k_{off}$ value, highlighting the key roles for more deeply buried residues in controlling both $k_{off}$ and the precision of substrate binding. The role of Ile-538 on helix 11 remains somewhat enigmatic because conversion to Ala reduces $k_{chem}$ by only 40%, whereas $k_{off}$ remains the same as WT; in this instance the bulk of the site chains at positions 500 and 839 may play a dominant role in the preservation of structure.

The kinetic observations for Trend III mutants are congruent with the finding of a previously described allosteric effect for WT SLO (31, 42, 43). In particular, the addition of oleic acid (mixed inhibitor) or OS (allosteric effector only) results in alleviation of the substrate-binding/reorientation steps as partial rate-determining steps (*i.e.* $^{D}k_{cat}/K_m = {}^{D}k_{cat}$) at low substrate concentration and reduced temperatures (31). Kinetic analysis supports a $k_{off}$ value that is ~60-fold faster in the presence of allosteric effector OS. HDX-MS analysis of the interactions of OS, which binds tightly ($K_D$ = ~0.6 μM) to an allosteric site and not in the active site substrate cavity of WT SLO, identified peptides within the N-terminal PLAT domain that had altered HDX properties (42). The implied conformational change is accompanied by a resolved network of peptides that exhibit enhanced peptidyl flexibility emanating from the PLAT domain to the substrate-binding portal (including helices 2 and 11). Thus, enhanced peptide flexibility within helices 2 and 11 also provides a structural basis for increased binding and release rates that arise from the addition of an allosteric effector.

Another recent temperature-dependent hydrogen–deuterium exchange study, comparing WT to I553X and L546A SLO variants, has implicated a role for Val-750 and Ile-552 within a catalytically linked protein network for communication between the HDX-identified thermally activated remote loop 317–334 and the active site (Fig. 3, *A* and *B*). Site-specific mutations within this remote loop have been shown to directly influence the enthalpic barrier for the chemical C–H bond activation step (25). This current study, together with the previous investigations of SLO, indicates the existence of distinct protein networks that modulate substrate-binding *versus* the subsequent bond cleavage steps. These networks consist of residues throughout separate regions of the protein scaffold, intersecting at Val-750 and Ile-552 (Fig. 3).

## Conclusion

The observed kinetic changes for 10 SLO mutants highlight the information content inherent in $^{D}k_{cat}/K_m$ regarding the mode of substrate binding in SLO. The origins of the more rate-limiting chemical steps for $k_{cat}/K_m$ in these mutants are seen to arise alternately from: (i) impairment of the precise substrate orientation in the binding site that leads to decreased rate constants of the initial chemical step, and (ii) increased flexibility of the substrate portal that increases the substrate-releasing step(s) in the case of V750A, I552A, I839A, and W500F. Significantly, these studies are able to define a network within SLO that proceeds from the surface substrate portal to the iron cofactor at the active site, although at the current level of understanding, we are unable to describe the details of the substrate movement and positioning within its binding channel. This work, which is based on classical enzymatic kinetic analyses, both deepens our understanding of where substrate binds and establishes a molecular framework for further structure function investigations. These studies are especially compelling, given the decades of effort that have failed to yield direct X-ray structural information regarding the E–S complex of SLO.

## Experimental procedures

### General information

All reagents were purchased from commercial sources and used without further purification unless otherwise indicated. H-LA (>99% purity) was purchased from Sigma–Aldrich and purified again before usage. D-LA for the competitive KIE measurements was isolated from the algal fatty acid mixture (Cambridge Isotope Laboratories, methyl esters U-D 97–98%, DLM-2491-0).

### Mutagenesis, expression, and purification of the SLO double mutants

Each lipoxygenase was expressed and purified as described previously (20, 41). Mutants were prepared following the Stratagene QuikChange Lightning protocol starting from the WT plasmid. The mutant plasmids were isolated and the mutants were confirmed by sequencing with three different primers that targeted different regions of the gene: the beginning of the gene,

a 500-bp region of the gene containing the mutation site(s), and a region that covers the 500-bp up to the end of the gene.

### *Kinetic measurement*

Steady-state kinetics was performed on a Cary50 spectrophotometer in the single-wavelength mode as previously described (20) (Table S1–S11).

### *Solvent viscosity studies*

The impact of viscosity on WT SLO, I552A, V750A, and L546A was determined at different relative viscosities ($\eta_{rel} = \eta/\eta^{\circ}$, where $\eta^{\circ}$ is the viscosity of $H_2O$ at 20 °C) as previously described (27). Buffer solutions of 0, 8, 14, 21.5, 26, and 30% by weight glucose in 0.1 M CHES buffer (pH 9.0) were prepared with corresponding relative viscosities of 1, 1.25, 1.5, 2.0, 2.5, and 3.0 at 20 °C. Enzymatic measurements at 20 °C were the same as described above. The enzymatic activities of WT SLO and three single mutants in 0.1 M CHES (pH 9.0) were found to be similar to those measured in 0.1 M borate buffer (pH 9.0).

### *Solvent isotope effects*

Solvent isotope effects for WT SLO, I552A, and L546A were obtained by comparing the kinetic parameters for protio-linoleic acid at 20 °C in 0.1 M borate (pH 9.0) in $D_2O$ (pH meter reading at 8.6) with those in $H_2O$ (pH 9.0). Because the relative viscosity of heavy water is 1.25, the solvent isotope effects on $k_{cat}/K_m$ needed to be corrected.

### *Isolation and purification of D-LA from an algal fatty acid ester mixture*

The algal fatty acid ester mixer (100 $\mu$l) was first de-esterified with 0.35 g of NaOH in ethanol (10 ml)/$H_2O$ (3.5 ml). After complete hydrolysis, the mixture was acidified by adding 65 ml of $H_2O$ and 1.5 ml of acetic acid followed by extraction with $CH_2Cl_2$ (5 ml performed four times). The extracted organic layer was dried to an oil, dissolved in methanol, and purified via RP-HPLC using Phenomenex semipreparative HPLC column (Luna C18, 100A, 250 mm × 10.00 mm, 5 $\mu$M) via isocratic elution (87.9% methanol, 12% $H_2O$, and 0.1% acetic acid) at a flow rate of 3 ml/min. The elution containing D-LA (with H-LA contamination) was collected, evaporated to oil, and further enzymatically treated with WT SLO to deplete the trace amount of H-LA contamination (monitored in the spectrophotometer, to ensure at least 10% substrate depletion) and then added acid, extracted, and dried as before. The post-enzymatic purified D-LA was dissolved in methanol and purified again via the semipreparative HPLC column via the same condition. The RP-HPLC purified D-LA was evaporated to dryness, dissolved in methanol, and stored at −80 °C.

### *Competitive kinetic isotope effect measurement*

The competitive KIEs ($^{D}k_{cat}/K_m$) for WT SLO, I552V, V750A, I538A, I839A, and W500F in 0.1 M borate (pH 9.0) between 10 and 40 °C were determined as previously described with some minor changes (30, 44). A known ratio of RP-HPLC–purified H- and D-LA (1:8; total concentration of the substrate, 10 $\mu$M) was allowed to react with individual SLO variants at the appropriate temperature. The reaction was monitored at 234 nm and stopped with acetic acid quench (final acetic acid concentration in the mixture of ~5%) at less than 3% total substrate consumption. The acidified reaction mixture is extracted with methylene chloride, evaporated to dryness, dissolved in methanol, and injected onto an analytic C18 column (Agilent, Purslt XRs 5 C18, 250 × 4.6 mm) and eluted at 1 ml/min with an isocratic mobile phase of 79.4% methanol, 21.5% $H_2O$, and 0.1% acetic acid. The molar protio/perdeutero-13(S)-hydroperoxy-9(Z),11(E)-octadecanoic acid (HPOD) ratios are equated to the corresponding peak area ratios, and the competitive KIE ($^{D}k_{cat}/K_m$) is calculated as $([P\text{-}H]/[P\text{-}D])_{+}/([P\text{-}H]/[P\text{-}D])_{\infty}$, where $([P\text{-}H]/[P\text{-}D])_{+}$ is the ratio of the integrated peak areas at <3% reaction conversion, and $([P\text{-}H]/[P\text{-}D])_{\infty}$ is the ratio of peak areas at complete conversion.

*Author contributions*—S. H. and J. P. K. conceptualization; S. H., A. R. O., E. D. L., and J. P. K. formal analysis; S. H. and J. P. K. writing-original draft; S. H., A. R. O., and J. P. K. writing-review and editing; J. P. K. supervision.

## References


1. Wolfenden, R., and Snider, M. J. (2001) The depth of chemical time and the power of enzymes as catalysts. *Acc. Chem. Res.* **34,** 938–945 CrossRef Medline
2. Michaelis, L., and Menten, M. L. (2013) The kinetics of the invertin action. 1913. *FEBS Lett.* **587,** 2712–2720 CrossRef Medline
3. Cleland, W. W., O'Leary, M. H., and Northrop, D. B. (1977) Isotope effects on enzyme-catalyzed reactions. In *Proceedings of the Sixth Annual Harry Steenbock Symposium*, held in Madison, Wisconsin, on June 4 and 5, 1976, University Park Press, Baltimore
4. Klinman, J. P. (1978) Kinetic isotope effects in enzymology. *Adv. Enzymol. Relat. Areas Mol. Biol.* **46,** 415–494 Medline
5. Klinman, J. P. (1977) Isotope effects in hydride transfer reactions. In *Sixth Steenbock Symposium on Isotope Effects on Enzyme Catalyzed Reactions* (Cleland, W. W., O'Leary, M. L., and Northrop, D. B., eds) University Park Press, Madison, Wisconsin
6. Klinman, J. P. (1978) Primary hydrogen isotope effects. In *Transition States of Biochemical Processes* (Gandour, R. D., and Schowen, R. L., eds) pp. 165–200, Plenum Press, New York
7. Cha, Y., Murray, C. J., and Klinman, J. P. (1989) Hydrogen tunneling in enzyme reactions. *Science* **243,** 1325–1330 CrossRef Medline
8. Allemann, R. K., and Scrutton, N. S. (2009) *Quantum Tunnelling in Enzyme-catalysed Reactions*, Royal Society of Chemistry, Cambridge, UK
9. Klinman, J. P., and Kohen, A. (2013) Hydrogen tunneling links protein dynamics to enzyme catalysis. *Annu. Rev. Biochem.* **82,** 471–496 CrossRef Medline
10. Klinman, J. P. (2013) Importance of protein dynamics during enzymatic C–H bond cleavage catalysis. *Biochemistry* **52,** 2068–2077 CrossRef Medline
11. Pudney, C. R., Guerriero, A., Baxter, N. J., Johannissen, L. O., Waltho, J. P., Hay, S., and Scrutton, N. S. (2013) Fast protein motions are coupled to enzyme H-transfer reactions. *J. Am. Chem. Soc.* **135,** 2512–2517 CrossRef Medline
12. Klinman, J. P. (2015) Dynamically achieved active site precision in enzyme catalysis. *Acc. Chem. Res.* **48,** 449–456 CrossRef Medline
13. Kohen, A. (2015) Role of dynamics in enzyme catalysis: substantial versus semantic controversies. *Acc. Chem. Res.* **48,** 466–473 CrossRef Medline
14. Porta, H., and Rocha-Sosa, M. (2002) Plant lipoxygenases: physiological and molecular features. *Plant Physiol.* **130,** 15–21 CrossRef Medline
15. Siedow, J. N. (1991) Plant lipoxygenase: structure and function. *Annu. Rev. Plant Physiol. Plant Mol. Biol.* **42,** 145–188 CrossRef
16. Jonsson, T., Glickman, M. H., Sun, S. J., and Klinman, J. P. (1996) Experimental evidence for extensive tunneling of hydrogen in the lipoxygenase

reaction: implications for enzyme catalysis. *J. Am. Chem. Soc.* **118,** 10319–10320 CrossRef
17. Knapp, M. J., Rickert, K., and Klinman, J. P. (2002) Temperature-dependent isotope effects in soybean lipoxygenase-1: correlating hydrogen tunneling with protein dynamics. *J. Am. Chem. Soc.* **124,** 3865–3874 CrossRef Medline
18. Hatcher, E., Soudackov, A. V., and Hammes-Schiffer, S. (2007) Proton-coupled electron transfer in soybean lipoxygenase: dynamical behavior and temperature dependence of kinetic isotope effects. *J. Am. Chem. Soc.* **129,** 187–196 CrossRef Medline
19. Meyer, M. P., Tomchick, D. R., and Klinman, J. P. (2008) Enzyme structure and dynamics affect hydrogen tunneling: the impact of a remote side chain (1553) in soybean lipoxygenase-1. *Proc. Natl. Acad. Sci. U.S.A.* **105,** 1146–1151 CrossRef Medline
20. Hu, S., Sharma, S. C., Scouras, A. D., Soudackov, A. V., Carr, C. A., Hammes-Schiffer, S., Alber, T., and Klinman, J. P. (2014) Extremely elevated room-temperature kinetic isotope effects quantify the critical role of barrier width in enzymatic C–H activation. *J. Am. Chem. Soc.* **136,** 8157–8160 CrossRef Medline
21. Glickman, M. H., and Klinman, J. P. (1996) Lipoxygenase reaction mechanism: demonstration that hydrogen abstraction from substrate precedes dioxygen binding during catalytic turnover. *Biochemistry* **35,** 12882–12892 CrossRef Medline
22. Hu, S., Cattin-Ortolá, J., Munos, J. W., and Klinman, J. P. (2016) Hydrostatic pressure studies distinguish global from local protein motions in C–H activation by soybean lipoxygenase-1. *Angew. Chem. Int. Ed. Engl.* **55,** 9361–9364 CrossRef Medline
23. Edwards, S. J., Soudackov, A. V., and Hammes-Schiffer, S. (2010) Impact of distal mutation on hydrogen transfer interface and substrate conformation in soybean lipoxygenase. *J. Phys. Chem. B* **114,** 6653–6660 CrossRef Medline
24. Klinman, J. P., and Offenbacher, A. R. (2018) Understanding biological hydrogen transfer through the lens of temperature dependent kinetic isotope effects. *Acc. Chem. Res.* **51,** 1966–1974 CrossRef Medline
25. Klinman, J. P., Offenbacher, A. R., and Hu, S. (2017) Origins of enzyme catalysis: experimental findings for C–H activation, new models, and their relevance to prevailing theoretical constructs. *J. Am. Chem. Soc.* **139,** 18409–18427 CrossRef Medline
26. Offenbacher, A. R., Hu, S., Poss, E. M., Carr, C. A. M., Scouras, A. D., Prigozhin, D. M., Iavarone, A. T., Palla, A., Alber, T., Fraser, J. S., and Klinman, J. P. (2017) Hydrogen–deuterium exchange of lipoxygenase uncovers a relationship between distal, solvent exposed protein motions and the thermal activation barrier for catalytic proton-coupled electron tunneling. *ACS Cent. Sci.* **3,** 570–579 CrossRef Medline
27. Glickman, M. H., and Klinman, J. P. (1995) Nature of rate-limiting steps in the soybean lipoxygenase-1 reaction. *Biochemistry* **34,** 14077–14092 CrossRef Medline
28. Newcomer, M. E., and Brash, A. R. (2015) The structural basis for specificity in lipoxygenase catalysis. *Protein Sci.* **24,** 298–309 CrossRef Medline
29. Coffa, G., Schneider, C., and Brash, A. R. (2005) A comprehensive model of positional and stereo control in lipoxygenases. *Biochem. Biophys. Res. Commun.* **338,** 87–92 CrossRef Medline
30. Sharma, S. C., and Klinman, J. P. (2015) Kinetic detection of orthogonal protein and chemical coordinates in enzyme catalysis: double mutants of soybean lipoxygenase. *Biochemistry* **54,** 5447–5456 CrossRef Medline
31. Mogul, R., Johansen, E., and Holman, T. R. (2000) Oleyl sulfate reveals allosteric inhibition of soybean lipoxygenase-1 and human 15-lipoxygenase. *Biochemistry* **39,** 4801–4807 CrossRef Medline
32. Minor, W., Steczko, J., Stec, B., Otwinowski, Z., Bolin, J. T., Walter, R., and Axelrod, B. (1996) Crystal structure of soybean lipoxygenase L-l at 1.4 angstrom resolution. *Biochemistry* **35,** 10687–10701 CrossRef Medline
33. Bradshaw, M. D., and Gaffney, B. J. (2014) Fluctuations of an exposed pi-helix involved in lipoxygenase substrate recognition. *Biochemistry* **53,** 5102–5110 CrossRef Medline
34. Gaffney, B. J., Bradshaw, M. D., Frausto, S. D., Wu, F., Freed, J. H., and Borbat, P. (2012) Locating a lipid at the portal to the lipoxygenase active site. *Biophys. J.* **103,** 2134–2144 CrossRef Medline
35. Tomchick, D. R., Phan, P., Cymborowski, M., Minor, W., and Holman, T. R. (2001) Structural and functional characterization of second-coordination sphere mutants of soybean lipoxygenase-1. *Biochemistry* **40,** 7509–7517 CrossRef Medline
36. Knapp, M. J., Seebeck, F. P., and Klinman, J. P. (2001) Steric control of oxygenation regiochemistry in soybean lipoxygenase-1. *J. Am. Chem. Soc.* **123,** 2931–2932 CrossRef Medline
37. Ruddat, V. C., Mogul, R., Chorny, I., Chen, C., Perrin, N., Whitman, S., Kenyon, V., Jacobson, M. P., Bernasconi, C. F., and Holman, T. R. (2004) Tryptophan 500 and arginine 707 define product and substrate active site binding in soybean lipoxygenase-1. *Biochemistry* **43,** 13063–13071 CrossRef Medline
38. Phatak, P., Venderley, J., Debrota, J., Li, J., and Iyengar, S. S. (2015) Active site dynamical effects in the hydrogen transfer rate-limiting step in the catalysis of linoleic acid by soybean lipoxygenase-1 (SLO-1): primary and secondary isotope contributions. *J. Phys. Chem. B* **119,** 9532–9546 CrossRef Medline
39. Horitani, M., Offenbacher, A. R., Carr, C. A., Yu, T., Hoeke, V., Cutsail, G. E., 3rd, Hammes-Schiffer, S., Klinman, J. P., and Hoffman, B. M. (2017) $^{13}$C ENDOR spectroscopy of lipoxygenase–substrate complexes reveals the structural basis for C–H activation by tunneling. *J. Am. Chem. Soc.* **139,** 1984–1997 CrossRef Medline
40. Hu, S., Offenbacher, A. R., Thompson, E. M., Gee, C. L., Wilcoxen, J., Carr, C. A. M., Prigozhin, D. M., Yang, V., Alber, T., Britt, R. D., Fraser, J. S., and Klinman, J. P. (2019) Biophysical characterization of a disabled double mutant of soybean lipoxygenase: the "undoing" of precise substrate positioning relative to metal cofactor and an identified dynamical network. *J. Am. Chem. Soc.* **141,** 1555–1567 CrossRef Medline
41. Hu, S., Soudackov, A. V., Hammes-Schiffer, S., and Klinman, J. P. (2017) Enhanced rigidification within a double mutant of soybean lipoxygenase provides experimental support for vibronically nonadiabatic proton-coupled electron transfer models. *ACS Catal.* **7,** 3569–3574 CrossRef Medline
42. Offenbacher, A. R., Iavarone, A. T., and Klinman, J. P. (2018) Hydrogen–deuterium exchange reveals long-range dynamical allostery in soybean lipoxygenase. *J. Biol. Chem.* **293,** 1138–1148 CrossRef Medline
43. Wecksler, A. T., Kenyon, V., Garcia, N. K., Deschamps, J. D., van der Donk, W. A., and Holman, T. R. (2009) Kinetic and structural investigations of the allosteric site in human epithelial 15-lipoxygenase-2. *Biochemistry* **48,** 8721–8730 CrossRef Medline
44. Lewis, E. R., Johansen, E., and Holman, T. R. (1999) Large competitive kinetic isotope effects in human 15-lipoxygenase catalysis measured by a novel HPLC method. *J. Am. Chem. Soc.* **121,** 1395–1396 CrossRef